Original Research

Amyloid Formation of Stefin B Protein Studied by Infrared Spectroscopy

Urban Novak[1], Eva Žerovnik[2], Ajda Taler-Verčič[2], MagdaTušek Žnidarič[3], Barbara Zupančič[1], Jože Grdadolnik[1],*

[1] Theory Department, National Institute of Chemistry, SI-1000 Ljubljana, Slovenia
[2] Department of Biochemistry and Molecular and Structural Biology, Jožef Stefan Institute, SI-1000 Ljubljana, Slovenia
[3] Department of Biotechnology and Systems Biology, National Institute of Biology, SI-1000 Ljubljana, Slovenia
*Correspondence: joze.grdadolnik@ki.si (Jože Grdadolnik)
Academic Editor: Guangyu Wu
Submitted: 23 December 2022   Revised: 1 February 2023   Accepted: 23 February 2023   Published: 6 March 2023

Abstract

Background: Stefin B, an established model protein for studying the stability and mechanism of protein folding, was used for monitoring protein aggregation and formation of amyloid structure by infrared spectroscopy. **Methods**: The analyses of the integral intensities of the low frequency part of the Amide I band, which is directly connected to the appearance of the cross-β structure reveals the temperature but not pH dependence of stefin B structure. **Results**: We show that pH value has significant role in the monomer stability of stefin B. Protein is less stable in acidic environment and becomes more stable in neutral or basic conditions. While in the case of the Amide I band area analysis we apply only spectral regions characteristic for only part of the protein in cross-β structure, the temperature study using multivariate curve resolution (MCR) analysis contains also information about the protein conformation states which do not correspond to native protein nor protein in cross-β structure. **Conclusions**: These facts results in the slightly different shapes of fitted sigmoid functions fitted to the weighted amount of the second basic spectrum (sc2), which is the closed approximation of the protein spectra with cross-β structure. Nevertheless, the applied method detects the initial change of the protein structure. Upon the analysis of infrared data a model for stefin B aggregation is proposed.

Keywords: stefin B; amyloid formation; infrared spectroscopy; aggregation; structure analysis

1. Introduction

Understanding the initialization and dynamic of protein aggregation is recognized as a key event in many studies of protein deposition diseases, protein folding, and protein drug stability. Although enormous efforts have been made to study amyloids and fibrils, the understanding of the early events during amyloid aggregation is still not satisfactory, although it seems to be crucial for identifying the mechanisms involved and for developing strategies to prevent and reverse amyloidogenic disorders [1]. Moreover, little is known about the structural changes underlying these processes. Infrared spectroscopy is one of the few techniques that can be efficiently used to determine the structure of proteins at the early aggregation stage. Among all techniques attenuated total reflectance spectroscopy (ATR) [2–5] is particularly suitable. By applying ATR the sample is examined on the surface of a highly reflective material such as ZnSe, diamond, or Ge. The use of single reflection ATR set up permits probing of protein solutions in water or in buffers with low solute concentration without saturation distortions of the most intense solvent bands [4]. Thus, the solvent spectra can be accurately subtracted and the analyses of the structure-sensitive protein bands become free from interference by the solvent bands.

Stefin B (cystatin B) is an established model protein for studying the stability and mechanism of protein folding [6,7] and for monitoring protein aggregation and amyloid fibrillation [7–12]. Human stefin B belongs to a family of proteins with an α/β secondary structure. It consists of 98 amino acids and is found in the cells both in the cytoplasm and in the lysosomes and nucleus. It shares its native topology, consisting of five β-strands surrounding a central α-helix with other cystatins [13]. Together with other stefins, it acts as an inhibitor of cysteine proteases [14,15]. Inhibition of cathepsins, specifically inhibition of cathepsin B, may partially explain the regulatory role of stefin B in the apoptosis process [16,17] and in cancer [18]. Stefin B can be found in its monomeric form in the cytosol [19], or as dimers [20] and as tetramers [21]. There is growing evidence that alternative functions are assigned to this small protein molecule. Stefin B appears as part of a multiprotein complex found in the cerebellum [22]. Overexpression of stefin B has been detected based on gene expression in amyotrophic lateral sclerosis [23] as well as in the primary immune response [24]. The pathological conditions observed in the stefin B-deficient mouse are apoptosis of nerve cells in the cerebellum, ataxia, as well as myoclonus [17]. Recent genetic studies link stefin B to progressive myoclonic epilepsy type 1 [25,26].

Human stefin B forms amyloid fibrils under *in vitro* conditions [10]. Stefin B fibrils possess all the properties attributed to all amyloid fibrils, i.e., long and relatively flat morphology, transverse β-diffraction pattern, specific staining with Congo red and the fluorescent dye thioflavin T, binding properties, and rigid core structure. During the long lag phase, granular aggregates form, which can be observed by transmission electron microscopy and dynamic light scattering [10,11,27,28]. The lag phase time can be accelerated by increasing the temperature, by adding 2,2,2-trifluoroethanol or by adding nuclei [21]. Different morphologies have been observed in the growth phase that follows the lag phase, but the morphology of aggregates in the steepest growth phase has not been fully elucidated [29]. Structure studies have shown that stefin B oligomers might form of domain swapping type [20]. The tetramers can be assumed to be the building blocks of the amyloid fibrils. However, the fibrillation reaction has shown that the formatted tetramer goes off-pathway and prevents fibril formation at higher protein concentrations [29]. Nowadays, a mixed fibril formation mechanism is proposed to cause the oligomerization and formation of fibrils of stefin B. The model involves both a nucleated polymerization and a conformational transformation at the nucleus. At a pH of 3.3 (isoelectric point od stefin B is 8.0), the reaction shows no lag phase, whereas at a pH of 4.8, a long lag phase is observed [8,9]. This is also the range where domain-swapping most likely occurs [29].

In this article we will demonstrate the ability of infrared spectroscopy to detect small protein structural changes induced by the temperature elevation. Moreover, by application of difference spectroscopy multivariate curve resolution and band fitting algorithm we may determine the early changes in protein structure which may induce the formation of the final aggregates. We varied pH and temperature to test the stability of stefin B against aggregation and to follow aggregation itself as a function of changes both external parameters.

2. Materials and Methods

2.1 Expression of Stefin B

Recombinant human stefin B protein (C3S, E31Y) was expressed in E. Coli [30,31]. Insulated and purified stefin B was dissolved in 0.05 M NaCl and stored as lyophilized powder.

2.2 Infrared Measurements

For infrared measurements lyophilized powder was dissolved in 0.1 M phosphate buffer to final concentration of 40 mg/mL. The appropriate pH values (3.0, 5.0, 7.5 and 9.0) of 0.1 M phosphate buffer was adjusted by using appropriate volumes of 0.1 M KH_2PO_4 and 0.1 M K_2HPO_4 buffer solutions. Sample with pH 3 was readjusted with HCl solution. Such solutions were filtered through 0.2 mm filter (Iso-Disc[TM], Sigma-Aldrich, Burlington, MA, USA),

which removed aggregates formed during the sample preparation. Filtered samples were stored on ice. The infrared spectra were measured by applying the Bruker Vertex 80 (Rosenheim, Germany) FTIR spectrometer. The Specac's Golden gate cell with diamond crystal and heated top plate was used for ATR measurements. Spectra were averaged from 64 interferograms in the range between 4000 and 500 cm^{-1}. Before analysis the spectrum of pure buffer (or water) was subtracted. We used difference spectroscopy to simplify recorded spectra. This spectroscopic method is sensitive to band-shape changes [32]. Changes in band-shapes caused by external perturbations are in complex spectra in general due to extensive band overlapping very difficult to evaluate. However, the proper subtraction of two consecutive spectra recorded at different temperature or different time, eliminates all undisturbed spectral feature, leaves visible only altered bands. Such kind of simplification of the recorded spectrum permits more adequate and accurate spectral analyses. The subtraction factor was determined by eliminating the bands that corresponds to the sidechain CH, CH_2, and CH_3 stretching vibrations (2800–3000 cm^{-1}) that are not affected by external perturbation. In addition, the band overlapping regions in spectra where only the solvent was subtracted were analyzed using the Grams/AI[TM] (Thermo Fisher Scientific, Waltham, MA, USA) band fitting program. The band shape of Amide I, II, and III was recalculated using model bands designed as mixed Lorentzian and Gaussian band shapes. The MCR approach for post-processing IR spectroscopic experimental data to investigate formation of aggregates is also used. MCR decompositions of the spectra (see **Supplementary Fig. 1**) which are composed of aggregates and non-aggregated protein molecules were performed using the Matlab software *MCR-ALS GUI v4c* [33,34] developed by the authors from Umea University, Sweden. The solution spectra of stefin B at various values of pH were measured in a temperature range from 25 °C to 75 °C. Backgrounds were collected at each recorded temperature to reduce the strong bands due to the absorption of diamond. The assignment of the structural sensitive band components in Amide I, II and III regions is based on structural studies on blocked dipeptides [35] and proteins in solution [36,37].

2.3 TEM

Lyophilized powder was dissolved in 0.1 M phosphate buffer (pH 5) to a final concentration of 1 mg/mL. Prepared sample was filtered through 0.2 mm filter (Iso-Disc[TM]) and incubated at 50 °C and 300 rpm for 96 h. Undiluted sample was applied to Formvar and carbon-coated grid (Agar Scientific, Stansted, UK) and left to adsorb for 3 min. The excess of sample was soaked away and stained with 1% (w/v) water solution of uranyl acetate. The excess of stain was removed immediately. The fibrils were observed with a Philips (Amsterdam, the Netherlands) CM 100 transmission electron microscope at 80 kV. Images were recorded

Table 1. The frequency-structure correlation table for the Amide I, II and III band components [37].

Conformation	Frequency (cm^{-1})		
	Amide I	Amide II	Amide III
turn	1664–1674	1563–1572	1257–1260
P_{II}	1648–1654	1543–1546	1308–1311
P_{II}-conformation	1634–1640	1560–1550	1308–1311
α-helix	1643–1645	1550–1552	1290–1295
α-conformation	1648–1654	1560–1550	1290–1295
β-conformation	1648–1654	1560–1550	1270–1280
β-strand	1625–1630	/	1240–1243
β-sheet	1685, 1630–1640	/	1230
aggregated β-sheets	1692, 1618	1530	1219–1222

Fig. 1. The spectrum of stefin B in the region with structural sensitive bands recorded at 25 °C and pH 7.5.

by Gatan Orius SC200 CCD camera and Digital Micrograph software 3.1, (Gatan Inc., Washington, DC, USA).

3. Results and Discussion

The region of proteins infrared spectra which possesses several characteristic bands, sensitive to protein conformation, expands between 1700 cm^{-1} and 1200 cm^{-1}. The most intense one is assigned as Amide I band. This mode involves mainly C=O stretching with small contributions of CN stretching, C$_\alpha$CN deformation and NH in-plane bending [38]. This composite nature of the Amide I mode leads to its sensitivity to various types of secondary structures. In addition to the complex potential energy distribution of Amide I mode, a C=O group acts as a proton acceptor and hence the frequency of Amide I band is also sensitive to formation of hydrogen bonds. The band fitting analysis revealed the complex band structure, which components were assigned the frequency-structure correlation of Amide I band proposed by Mirtič and Grdadolnik [37]. These correlations were evaluated on the basis of the structural study of poly-L-lysine peptide and are shown in the Table 1 (Ref. [37]).

The second most intense peak from the Fig. 1 belongs to Amide II mode. The Amide II mode is led by NH in-plane bending and CN stretching. Other contributions to this mode are C$_\alpha$C stretching, C=O in-plane bending and N$_\alpha$C stretching [38]. Since the largest contribution to this mode is the NH in-plane bending, the Amide II band is very sensitive to formation of the hydrogen bond, where NH proton acts in the role of a proton donor. The frequency dependence of Amide II shown in Table 1 indicates that it is more sensitive to the strength of hydrogen bonds than to the various types of secondary structures.

In the vicinity of Amide II band side-chain region appears. In the spectrum of stefin B two characteristic groups of bands one culminated near 1450 cm^{-1} and the second one near 1400 cm^{-1} can be observed. These bands originate from the modes of the side-chains, such as the deformation modes of the CH$_2$ and CH$_3$ groups or the symmetric stretching of the ionized COO$^-$ groups, which is gen-
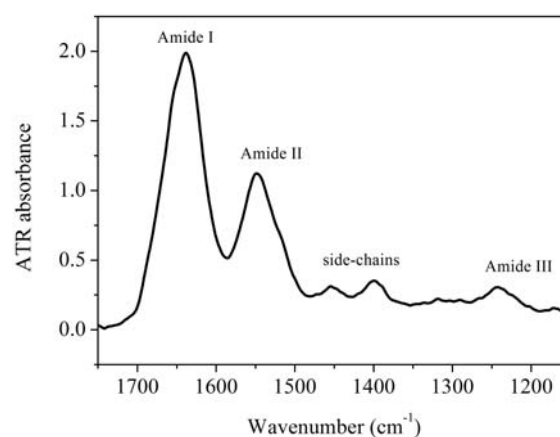
erally near 1400 cm^{-1} [39]. The Amide III region ends the infrared spectrum of stefin B presented in the Fig. 1. It appears as less intensive but complex band between 1320 cm^{-1} and 1220 cm^{-1}. In-plane NH bending, coupled with some other peptide modes (CN stretching, CC stretching, and CO in-plane), is the main contributor to the Amide III mode [38,40]. The conformational sensitivity of the Amide III components has been tested by numerous experimental and theoretical studies [38]. These studies show that the frequency of the Amide III besides the different type of secondary structure depends also on both dihedral angles of amino acid residues.

The applicability of infrared spectroscopy for monitoring protein aggregation lay in the temperature measurement of protein solutions. From the assignment of the band components of the Amide I band (Table 1) it is evident that the low-frequency components originate in protein aggregation. The Amide I band frequencies of the aggregated protein are much lower even compared to the Amide I band frequencies characteristic of the β-sheet population. Thus, the protein aggregation caused by the temperature increase increases the intensity of the low-frequency component shown in Fig. 2. The increase of the intensity can be simply followed by the integration of the low frequency part of the Amide I band in the region 1627 cm^{-1} and 1600 cm^{-1}. The typical temperature of monomer to aggregate transition correlates with the pH values. It starts at 48 °C at pH 3.0, followed by 53 °C at pH 5.0, and by 61 °C at pH 7.5 to reach the final value of 63 °C at pH 9.0. It is obvious that higher pH values structurally stabilize the monomeric protein and make aggregation more difficult. So the difference in transition temperature depends on which side of the isoelectric point of the protein the experiment is performed. The isoelectric point of stefin B is 8.0, and the difference between the transition temperature directly below and above the isoelectric point is 8°, while the pH variation on a same side of isoelectric point (below or above) changes the transition temperature by 5° and 2°, respectively. As expected,
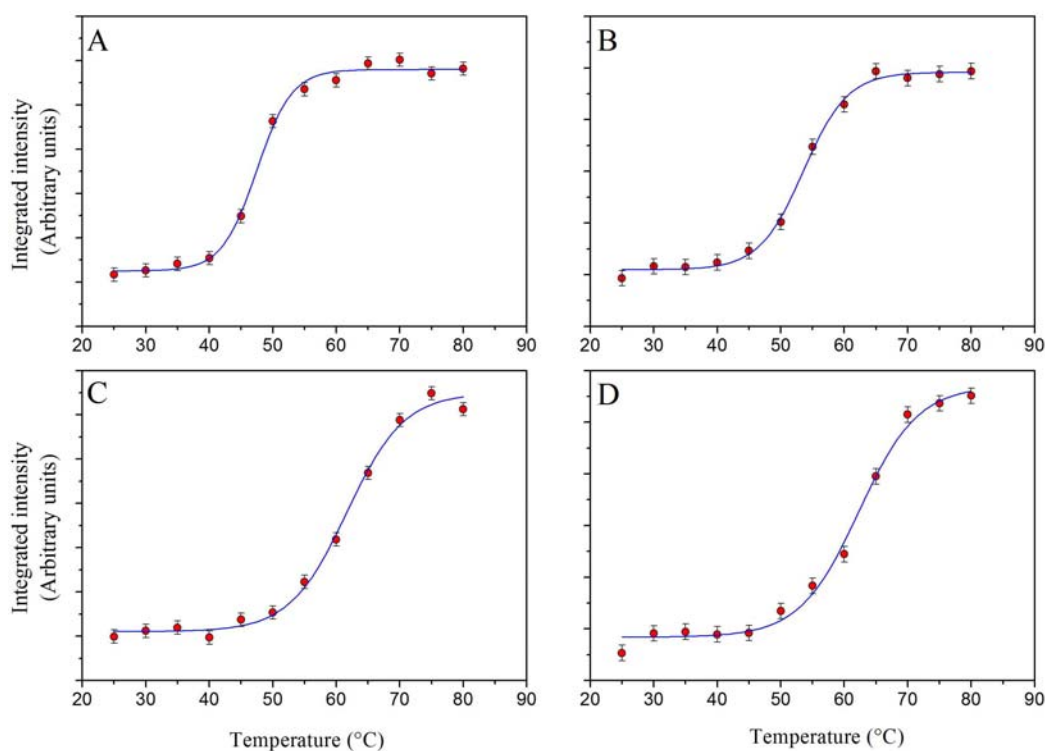
Fig. 2. The variation of the integral intensity of the Amide I band in the region between 1627 cm^{-1} and 1600 cm^{-1} as a function of temperature. pH values of stefin B solutions were: (A) pH 3; (B) pH 5; (C) pH 7.5 and (D) pH 9.

protein aggregation is related to the amount and distribution of electric charge on the protein surface.

The changes in protein bands in the central region of the protein spectrum upon heating were further investigated by difference spectroscopy. In the Fig. 3 (and **Supplementary Figs. 2,3,4**) typical difference spectra are shown. The difference spectrum presented in Fig. 3B is calculated at the beginning of the heating process. In the case of stefin B at pH 3, the spectrum recorded at 30 °C was subtracted from the spectrum recorded at 40 °C. It is worth noting that the initial difference spectrum (Fig. 3B) is different compared to the ones recorded at higher temperatures. It is worth noting that the initial difference spectrum (Fig. 3B) is different compared to the ones recorded at higher temperatures. While in the other two (C and D for Fig. 2 and **Supplementary Figs. 2,3,4**), as expected, the main feature is observed in the Amide I region due to the increase in aggregated protein, in the initial difference spectrum the change in the Amide II region is the most intense one. The negative band located at higher frequency is red-shifted upon heating. Since the NH deformation is the main constituent of Amide II mode, the origin of frequency red-shift is weakening of the hydrogen bonds where NH groups from the backbone act as a proton donor. The spectral changes in the Amide I and III regions are less impressive. The only exception is the low frequency component of Amide III band which is already noticeable and its appearance indicates structural changes due to protein aggregation. Struc-

tural changes which will be studied in details by band fitting algorithm are more visible in the last two difference spectra. The formation of the fibrils, as will be approved later on with electron microscopy, is noticeable by the appearance of intense positive band at 1623 cm^{-1} as a part of Amide I.

Information obtained by difference spectroscopy (indications of band composition such as number of peaks with approximate peak frequencies) was used to model intrinsic bands in a method of band decomposition. In general, the method of band decomposition, which results are shown in the Fig. 4 and in the **Supplementary Fig. 5**, has several drawback, it presents the only way how to quantitatively evaluate conformational changes due to aggregation triggered by the increase of the temperature. The crucial part of the optimization process, i.e., the setting of the initial band parameters (number, position and relative intensity) were derived from three independent methods; difference spectroscopy, deconvolution and second derivative spectroscopy.

It is well known that the accuracy of this kind of spectral decomposition is severely limited. Even if the assignment is not problematic, the proposed combination of intrinsic bands and integrated intensities used for quantitative interpretation may not be unique. However, in the case of protein spectra, we have two overlapping regions, Amide I and Amide III, which should contain the same information about the secondary structure. Therefore, we significantly reduce the number of possible band combinations
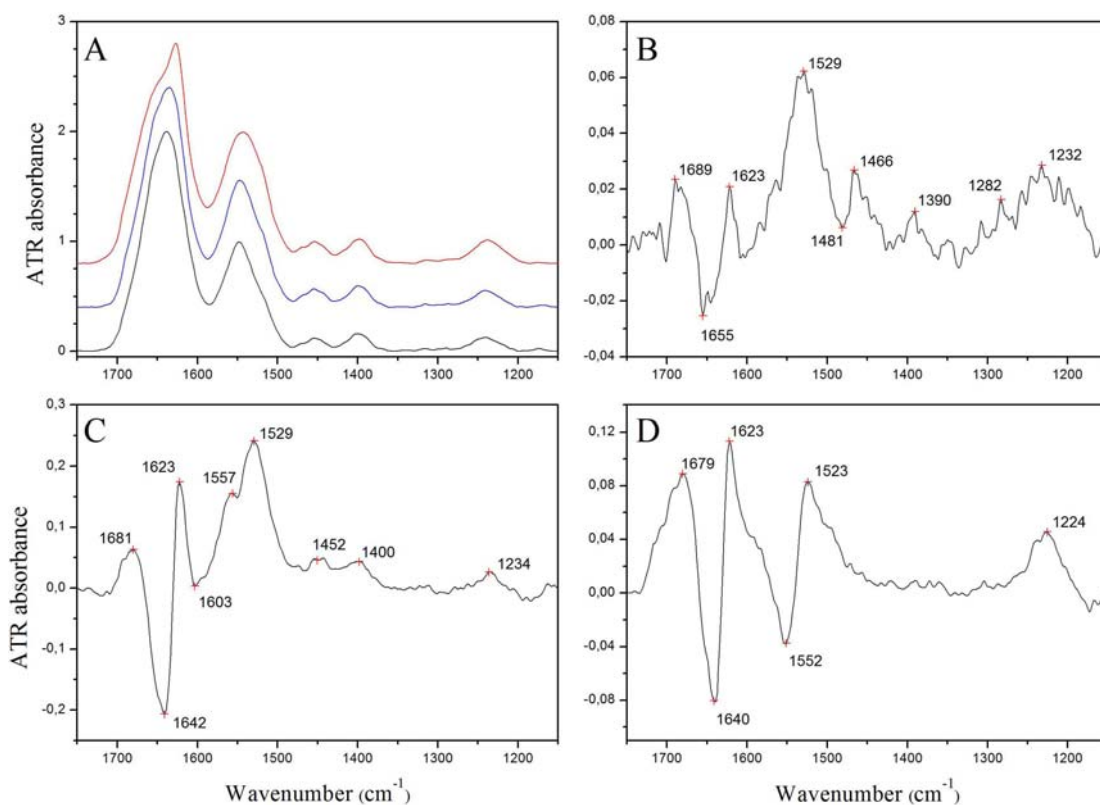
Fig. 3. Temperature dependent spectra of stefin B with corresponding difference spectra. (A) Spectra recorded at pH 3 and at different temperatures (Black 30°C, blue 45°C and red 65°C). Solvent was subtracted. (B) Difference spectrum: 40°C–30°C. (C) Difference spectrum: 50°C–40°C in (D) difference spectrum: 65°C–50°C.

that could satisfactorily match the experimental spectrum. We used only the band combinations for which the agreement between the secondary structure predictions from both regions, Amide I and Amide III, respectively, is relevant. The error is still large, but we obtain a consistent picture of the structural changes caused by temperature or changing pH value.

By comparison of the secondary structure predicted from the Amide I and Amide III composition, it is evident that pH value does not have noticeable influence the secondary structure of stefin B. The population of α-helices is about 20%, while the population of β-sheets is about 40%. Analysis of both regions gives slightly different population, however when we take into account that in analysis of α-helices by applying Amide III region we are able to distinguish amino acids, which are a part of α-helices and those which are not but still in α-conformation the matching is even better. The situation is similar for the β-sheet determination, where the amide III analysis finds some aggregates that are already present at the lowest measured temperatures.

Results summarized in Table 2 evidently show that aggregation at all probed pH values significantly changes the secondary structure of the protein. The band at 1230 cm^{-1}, which is assigned to β-sheet structure loses the intensity while on contrary the band at lower frequency, indicative

for cross-β structure, increases the intensity. These conformational changes are also indicated by the intensity variations of the Amide III band components at 1230 cm^{-1} and 1220 cm^{-1}, respectively. It is worth to note, that partially aggregated proteins exist already at 25 °C at all pH values. The population is small (approx. 4%) but noticeable (Tables 2,3).

The decomposition of Amide I and III bands shows that aggregation affects the protein structure is not pH dependent. Besides the mentioned differences in protein structure, the increase of the temperature slightly changes also the populations of α, β, and P$_{II}$ conformers. For detailed structural changes of particular conformation see the Tables 2,3. It is also noticeable that at higher temperatures not all proteins are part of cross-β structures. At all pH values, a rather large population of β-sheets is found (6%–13%), possibly belonging to monomeric proteins that are still present at higher temperatures. More interesting is the population of β-strands, which increases with heating. The appearance of this conformation may be the result of partial unfolding during the formation of a cross-β structure.

We have applied another mathematical method, which verified significantly reduce the complexity of the vibrational spectra. MCR decomposition finds orthogonal spectra using only one constraint; the spectral components should not contain any negative bands. The results of such
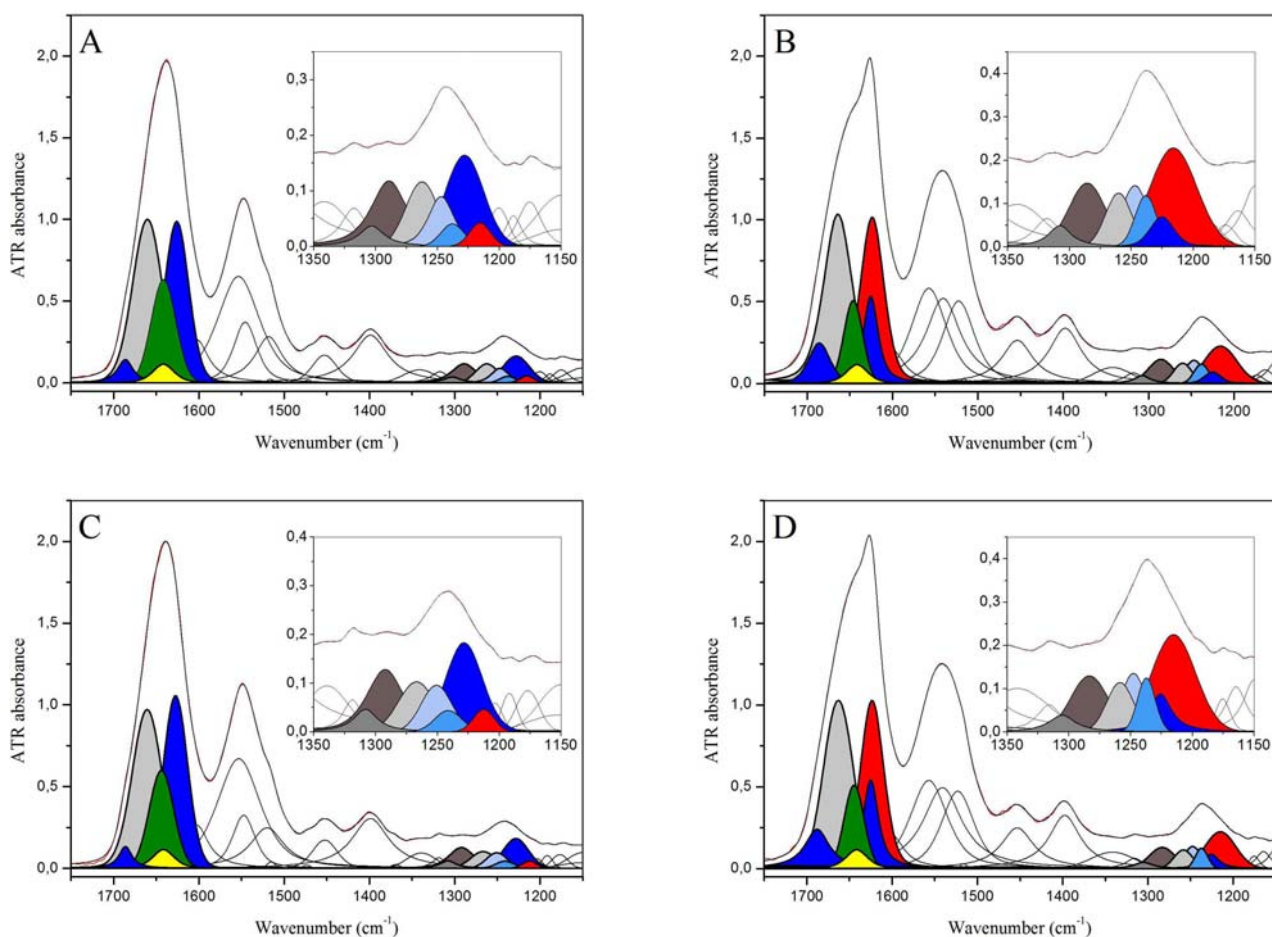
Fig. 4. Band structure of the Amide I, II, and III region of stefin B optimised by the band fitting algorithm. (A) pH 3 at T = 25 °C; (B) pH 3 at T = 70 °C; (C) pH 5 at T = 25 °C and (D) pH 5 at T = 70 °C.
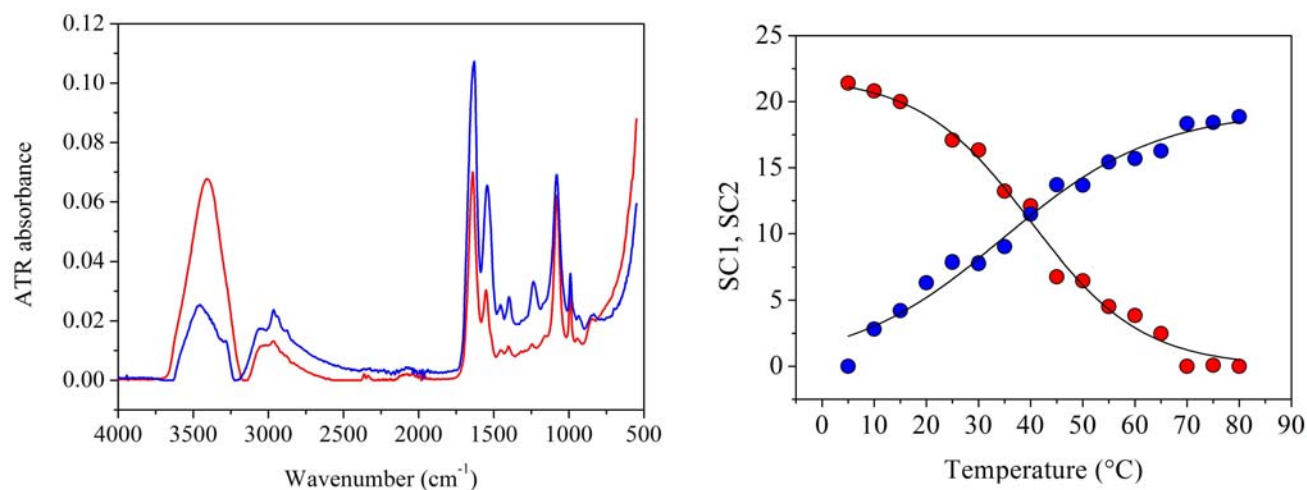

Fig. 5. Decomposition of the temperature dependent spectra of stefin B at pH 7.5. (Left) sc1 (blue spectrum) and sc2 (red spectrum) components retrieved from the MCR procedure. (Right) the participation (weights) of both components in raw spectra. Raw spectra were recorded at pH 7.5.

decomposition of the temperature dependent stefin B at pH 7.5 are shown in Fig. 5. For other pH value decompositions are presented in Supplementary file (**Supplementary**

Figs. 6,7,8,9). Two spectral components were found that cover more than 99% of the spectral variance in the series of temperature measurements at given pH value. Simpli-

Table 2. The summary of the conformational changes observed by analysis of the Amide I and Amide III region by applying band fitting algorithm; pH 3.0 and pH 5.0.

Mode	pH 3.0				Assignment	pH 5.0			
	(cm^{-1})	$T = 25\,^\circ\text{C}$ (%)	$T = 70\,^\circ\text{C}$ (%)	(cm^{-1})		(cm^{-1})	$T = 25\,^\circ\text{C}$ (%)	$T = 70\,^\circ\text{C}$ (%)	(cm^{-1})
	1686	4	7	1686	β-sheet	1686	3	9	1688
	1660	41	39	1664	turns, loops	1661	41	35	1663
Amide I	1641	21	11	1646	α-helix	1644	20	12	1645
	1626	34	12	1625	β-sheet	1627	36	13	1625
	1620	0	31	1623	β-sheet agg.	1620	0	31	1623
	1303	6	6	1308	P_{II}	1308	7	5	1305
	1289	26	19	1286	α	1292	26	17	1283
	1262	17	11	1260	β_{120}	1267	16	11	1258
Amide III	1247	13	16	1247	β_{150}	1251	12	15	1248
	1238	5	8	1238	β-strand	1241	5	8	1237
	1228	29	6	1225	β-sheet	1228	30	9	1226
	1215	4	34	1216	β-sheet agg.	1212	4	35	1215

Table 3. The summary of the conformational changes observed by analysis of the Amide I and Amide III region by applying band fitting algorithm; pH 7.5 and pH 9.0.

Mode	pH 7.5				Assignment	pH 9.0			
	(cm^{-1})	$T = 25\,^\circ\text{C}$ (%)	$T = 70\,^\circ\text{C}$ (%)	(cm^{-1})		(cm^{-1})	$T = 25\,^\circ\text{C}$ (%)	$T = 70\,^\circ\text{C}$ (%)	(cm^{-1})
	1687	3	12	1688	β-sheet	1686	4	12	1687
	1661	41	34	1662	turns, loops	1660	41	34	1662
Amide I	1643	19	10	1645	α-helix	1643	19	12	1645
	1627	37	12	1625	β-sheet	1627	36	11	1625
	1620	0	32	1623	β-sheet agg.	1620	0	31	1622
	1305	8	6	1306	P_{II}	1302	6	6	1308
	1290	26	14	1285	α	1289	25	16	1284
	1265	15	11	1261	β_{120}	1264	16	11	1261
Amide III	1248	13	13	1248	β_{150}	1251	13	11	1249
	1239	5	9	1240	β-strand	1240	5	11	1240
	1228	29	11	1230	β-sheet	1230	31	9	1228
	1217	4	36	1218	β-sheet agg.	1219	4	36	1222

Table 4. The most intense infrared bands from the component spectra of sc1 and sc2.

Band assignment	Component	pH 5.0	pH 7.5	pH 9.0
OH, NH stretchings	sc1	3397	3404	3409
	sc2	3463, 3281	3454, 3283	3450, 3288
Amide I	sc1	1639	1641	1640
	sc2	1628	1629	1628
Amide II	sc1	1551	1550	1551
	sc2	1543	1544	1542
Amide III	sc1	1246	1245	1244
	sc2	1235	1234	1234

fication of the spectra is expecially valuable in the regions where strong overlapping occurs. One of this is Amide I and III band regions, which frequencies of intrinsic bands can be attributed to the various protein structures (Table 2). Indeed we found differences in the band frequencies of both Amide bands in sc1 and sc2 components, which have been calculated as the orthogonal basis for particular temperature measurements at various pH values (Table 4).

The spectral components and especially the frequencies of the most prominent bands in these spectra show that these two spectra are still complex and do not represent the pure native and aggregated state. While the first sc1 spectral component is relatively close to the spectrum of native stefin B, the sc2 spectral component is obviously the superposition of slightly distorted protein and protein with the cross-β elements. The sc2 band components attributable to the amide I, II, and III bands change frequencies toward values characteristic of the cross-β structure but remain somewhat higher. Therefore, this spectral component also seems to contain the information of the conformational state that lies between the native and the aggregated protein. It is also informative that almost no changes in other types of secondary structures are observed, supporting the hypothesis that the aggregation process involves only the redirection of
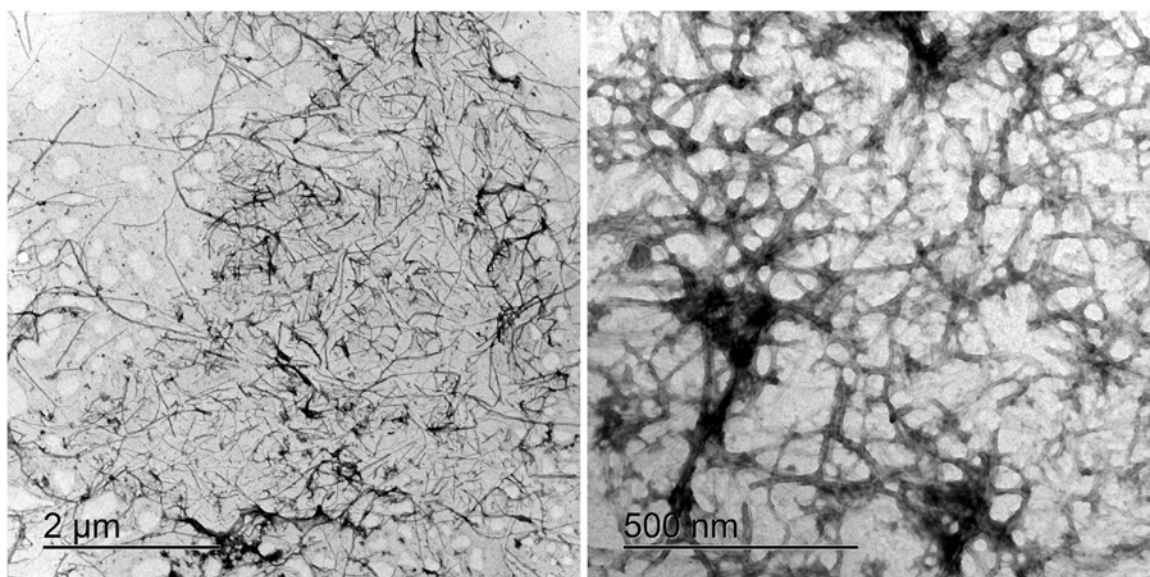
Fig. 6. TEM images of stefin B aggregates recorded 96 hours after the initiation of aggregation process. Stefin B was dissolved in 0.1 M phosphatic buffer at pH 5.0.
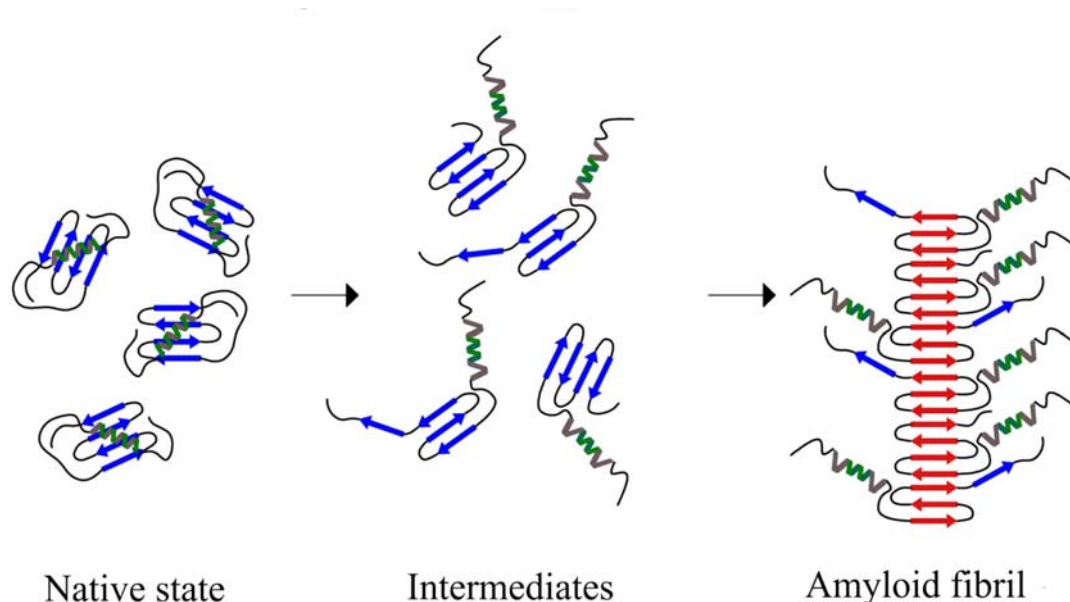

Fig. 7. Proposed model of stefin B amyloid fibril formation, which was prepared based on the data obtained with FTIR spectroscopy.

the secondary elements (β-sheets), which is followed by the formation of the cross-β structure. This is also true for the formation of the β-strands with their characteristic bands in the amide region III (Tables 2,3). As expected, the application of the band fitting procedure provided the most detailed information. However, the results of the MCR analysis suggest that in addition to the two structures, native and aggregated with cross-β structure; there is another one that connects the two. And this third structure can be classified as the intermediates.

The aggregation and the types of aggregates were additionally verified by applying microscopy. Imaging of the amyloid fibrils was done using TEM. TEM was applied at the final stages of fibril growth as used in the infrared experiments. In Fig. 6 stefin B amyloid fibrils at pH 5.0 are shown. Aggregates have regular, smooth morphology with the compliance to amyloid fibrils morphology.

Based on the data obtained with FTIR spectroscopy (quantitative data shown in Tables 2,3) we propose a new model of stefin B amyloid fibril formation (Fig. 7). Inter-

mediates are partially unfolded secondary structures, where α-helix is partially unfolded and some hydrogen bonds between molecular groups of the main polypeptide chain are broken. The core of amyloid fibrils is formed from native state's β-strands (3 or 4 strands form the core), which, in the process of amyloid fibril formation, form a cross-β structure. Around the fibril core α-helixes and some β-strands are placed. Native state is represented by four β-strands which form one β-sheet. Intermediates have partially unfolded secondary elements, where α-helices, as well as, β-sheets are partially unfolded. At the same time some hydrogen bonds between molecular groups of the main polypeptide chain are broken. At last step amyloid fibrils are formed. Theirs core is formed from native state's β-strands, which, in the process of amyloid fibril formation, form a cross-β structure. This is in a slight contradiction with the band fitting analysis where some minor decrease of population of the α-helix structures were observed, which can be ascribed by the partial unfolding of the ends of α-helices.

4. Conclusions

Stefin B represents ideal protein with characteristic α/β structure as a tester for elucidating the applicability of the infrared spectroscopy to detect delicate changes in protein structure which are connected to early stages of protein aggregation. We used two different approaches to rationalize the spectral changes in amides bands and correlate these band perturbations to protein aggregation. Difference spectroscopy gives the details in changes of amides band shapes and frequencies. The detection of the low frequency components serves as an indicator for formation of the cross-β structure and thus aggregation and formation of the fibrils. Additional to analysis of the Amide I bands, Amide III reveals even more detailed structural information. Besides the changes of the secondary structure we get also the overview about the protein parts which are not part of organized and well-structured protein. The low frequency part of the Amide I bands nicely reproduce the phase transition from monomer protein to aggregated suspension of proteins in characteristic cross-β pattern. We showed that pH value has no impact on the protein structure. However, it strongly influences on the protein stability. In the acidic environment the temperature of formation of aggregates is determined at 48 °C while at the highest pH value it reaches to 63 °C. The elevation of the typically temperature of formation of aggregates implies that basicity of environment protect stefin B from formation of the amyloidal fibrils. The proposed model of formation of stefin B amyloids was constructed on the basis of analysing infrared temperature measurements with difference spectroscopy, band fitting algorithm and MCR analysis.

Availability of Data and Materials

The data presented in this study are available on request from the corresponding author.

Author Contributions

Conceptualization—UN, BZ, EŽ, ATV, MTŽ and JG; methodology—UN, BZ, EŽ, ATV, MTŽ and JG; validation—UN, BZ, EŽ, ATV, MTŽ and JG; formal analysis—UN, BZ, EŽ, ATV, MTŽ and JG; data curation—UN, BZ, EŽ, ATV, MTŽ and JG; writing - original draft preparation—UN and JG; writing - review and editing—UN and JG; visualization—UN and JG; supervision—JG; funding acquisition—JG.

Ethics Approval and Consent to Participate

Not applicable.

Acknowledgment

Not applicable.

Conflict of Interest

The authors declare no conflict of interest. ATV and EŽ are serving as the Guest editors of this journal. We declare that ATV and EŽ had no involvement in the peer review of this article and has no access to information regarding its peer review.

Supplementary Material

Supplementary material associated with this article can be found, in the online version, at https://doi.org/10.31083/j.fbl2803046.

References

[1] Chiti F, Dobson CM. Protein Misfolding, Amyloid Formation, and Human Disease: A Summary of Progress Over the Last Decade. Annual Review of Biochemistry. 2017; 86: 27–68.

[2] Vigano C, Manciu L, Buyse F, Goormaghtigh E, Ruysschaert JM. Attenuated total reflection IR spectroscopy as a tool to investigate the structure, orientation and tertiary structure changes in peptides and membrane proteins. Biopolymers. 2000; 55: 373–380.

[3] Harrick NJ. Internal Reflection Spectroscopy. John Wiley & Sons: NJ, USA. 1987.

[4] Grdadolnik J. Saturation Effects in FTIR Spectroscopy: Investigation of Amide I and Amide II Bands in Protein Spectra. Acta Chimica Slovenica. 2003; 50: 777–788.

[5] Grdadolnik J. ATR-FTIR Spectroscopy: Its Advantages and limitations. Acta Chimica Slovenica. 2002; 49: 631–642.

[6] Zerovnik E, Jerala R, Virden R, Kroon Zitko L, Turk V, Waltho JP. On the mechanism of human stefin B folding: II. Folding from GuHCl unfolded, TFE denatured, acid denatured, and acid intermediate states. Proteins. 1998; 32: 304–313.

[7] Zerovnik E, Virden R, Jerala R, Turk V, Waltho JP. On the mechanism of human stefin B folding: I. Comparison to homologous stefin A. Influence of pH and trifluoroethanol on the fast and slow folding phases. Proteins. 1998; 32: 296–303.

[8] Žerovnik E, Stoka V, Mirtič A, Gunčar G, Grdadolnik J, Staniforth RA, *et al*. Mechanisms of amyloid fibril formation–focus on domain-swapping. The FEBS Journal. 2011; 278: 2263–2282.

[9] Zerovnik E. Amyloid-fibril formation. Proposed mechanisms and relevance to conformational disease. European Journal of Biochemistry. 2002; 269: 3362–3371.

[10] Zerovnik E, Pompe-Novak M, Skarabot M, Ravnikar M, Musevic I, Turk V. Human stefin B readily forms amyloid fibrils *in vitro*. Biochimica et Biophysica Acta. 2002; 1594: 1–5.

[11] Zerovnik E, Skarabot M, Skerget K, Giannini S, Stoka V, Jenko-Kokalj S, *et al*. Amyloid fibril formation by human stefin B: influence of pH and TFE on fibril growth and morphology. Amyloid: the International Journal of Experimental and Clinical Investigation: the Official Journal of the International Society of Amyloidosis. 2007; 14: 237–247.

[12] Zerovnik E, Staniforth RA, Turk D. Amyloid fibril formation by human stefins: Structure, mechanism & putative functions. Biochimie. 2010; 92: 1597–1607.

[13] Morgan GJ, Giannini S, Hounslow AM, Craven CJ, Zerovnik E, Turk V, *et al*. Exclusion of the native alpha-helix from the amyloid fibrils of a mixed alpha/beta protein. Journal of Molecular Biology. 2008; 375: 487–498.

[14] Turk V, Bode W. The cystatins: protein inhibitors of cysteine proteinases. FEBS Letters. 1991; 285: 213–219.

[15] Turk V, Turk B, Turk D. Lysosomal cysteine proteases: facts and opportunities. The EMBO Journal. 2001; 20: 4629–4633.

[16] Houseweart MK, Pennacchio LA, Vilaythong A, Peters C, Noebels JL, Myers RM. Cathepsin B but not cathepsins L or S contributes to the pathogenesis of Unverricht-Lundborg progressive myoclonus epilepsy (EPM1). Journal of Neurobiology. 2003; 56: 315–327.

[17] Pennacchio LA, Bouley DM, Higgins KM, Scott MP, Noebels JL, Myers RM. Progressive ataxia, myoclonic epilepsy and cerebellar apoptosis in cystatin B-deficient mice. Nature Genetics. 1998; 20: 251–258.

[18] Kos J, Krasovec M, Cimerman N, Nielsen HJ, Christensen IJ, Brünner N. Cysteine proteinase inhibitors stefin A, stefin B, and cystatin C in sera from patients with colorectal cancer: relation to prognosis. Clinical Cancer Research: an Official Journal of the American Association for Cancer Research. 2000; 6: 505–511.

[19] Alakurtti K, Weber E, Rinne R, Theil G, de Haan GJ, Lindhout D, *et al*. Loss of lysosomal association of cystatin B proteins representing progressive myoclonus epilepsy, EPM1, mutations. European Journal of Human Genetics. 2005; 13: 208–215.

[20] Jerala R, Zerovnik E. Accessing the global minimum conformation of stefin A dimer by annealing under partially denaturing conditions. Journal of Molecular Biology. 1999; 291: 1079–1089.

[21] Jenko S, Skarabot M, Kenig M, Guncar G, Musevic I, Turk D, *et al*. Different propensity to form amyloid fibrils by two homologous proteins-Human stefins A and B: searching for an explanation. Proteins. 2004; 55: 417–425.

[22] Di Giaimo R, Riccio M, Santi S, Galeotti C, Ambrosetti DC, Melli M. New insights into the molecular basis of progressive myoclonus epilepsy: a multiprotein complex with cystatin B. Human Molecular Genetics. 2002; 11: 2941–2950.

[23] Malaspina A, Kaushik N, de Belleroche J. Differential expression of 14 genes in amyotrophic lateral sclerosis spinal cord detected using gridded cDNA arrays. Journal of Neurochemistry. 2001; 77: 132–145.

[24] Lefebvre C, Cocquerelle C, Vandenbulcke F, Hot D, Huot L, Lemoine Y, *et al*. Transcriptomic analysis in the leech Theromyzon tessulatum: involvement of cystatin B in innate immunity. The Biochemical Journal. 2004; 380: 617–625.

[25] Pennacchio LA, Lehesjoki AE, Stone NE, Willour VL, Virtaneva K, Miao J, *et al*. Mutations in the gene encoding cystatin B in progressive myoclonus epilepsy (EPM1). Science. 1996; 271: 1731–1734.

[26] Lalioti MD, Scott HS, Buresi C, Rossier C, Bottani A, Morris MA, *et al*. Dodecamer repeat expansion in cystatin B gene in progressive myoclonus epilepsy. Nature. 1997; 386: 847–851.

[27] Jenko Kokalj S, Guncar G, Stern I, Morgan G, Rabzelj S, Kenig M, *et al*. Essential role of proline isomerization in stefin B tetramer formation. Journal of Molecular Biology. 2007; 366: 1569–1579.

[28] Ceru S, Kokalj SJ, Rabzelj S, Skarabot M, Gutierrez-Aguirre I, Kopitar-Jerala N, *et al*. Size and morphology of toxic oligomers of amyloidogenic proteins: a case study of human stefin B. Amyloid. 2008; 15: 147–159.

[29] Skerget K, Vilfan A, Pompe-Novak M, Turk V, Waltho JP, Turk D, *et al*. The mechanism of amyloid-fibril formation by stefin B: temperature and protein concentration dependence of the rates. Proteins. 2009; 74: 425–436.

[30] Rabzelj S, Turk V, Zerovnik E. *In vitro* study of stability and amyloid-fibril formation of two mutants of human stefin B (cystatin B) occurring in patients with EPM1. Protein Science. 2005; 14: 2713–2722.

[31] Jerala R, Trstenjak M, Lenarcic B, Turk V. Cloning a synthetic gene for human stefin B and its expression in E. coli. FEBS Letters. 1988; 239: 41–44.

[32] Grdadolnik J. Infrared Difference Spectroscopy: Part I. Interpretation of the Difference Spectrum. Vibrational Spectroscopy. 2003; 31: 279–288.

[33] MCR-ALS GUI v4c, Umeå Univ. Sweden. 2016. Available at: https://www.umu.se/en/research/infrastructure/visp/downloads/ (Accessed: 18 November 2020).

[34] Gorzsás A. Vibrational Spectroscopy Core Facility, Umeå Univ. Sweden. 2016. Available at: https://www.umu.se/en/research/infrastructure/visp/downloads/ (Accessed: 21 October 2020).

[35] Grdadolnik J, Mohacek-Grosev V, Baldwin RL, Avbelj F. Populations of the three major backbone conformations in 19 amino acid dipeptides. Proceedings of the National Academy of Sciences of the United States of America. 2011; 108: 1794–1798.

[36] Grdadolnik J, Maréchal Y. Bovine serum albumin observed by infrared spectrometry. I. Methodology, structural investigation, and water uptake. Biopolymers. 2001; 62: 40–53.

[37] Mirtič A, Grdadolnik J. The structure of poly-L-lysine in different solvents. Biophysical Chemistry. 2013; 175–176: 47–53.

[38] Krimm S. Interpreting Infrared Spectra of Peptides and Proteins. In Infrared Analysis of Peptides and Proteins. American Chemical Society.1999; 750: 38–53.

[39] Barth A. The infrared absorption of amino acid side chains. Progress in Biophysics and Molecular Biology. 2000; 74: 141–173.

[40] Grdadolnik J, Grdadolnik SG, Avbelj F. Determination of conformational preferences of dipeptides using vibrational spectroscopy. The Journal of Physical Chemistry. B. 2008; 112: 2712–2718.